

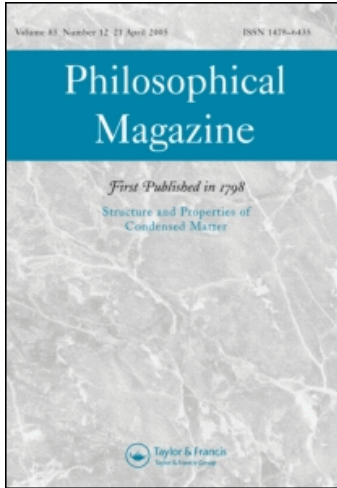
This article was downloaded by: [Monash University]

On: 28 January 2010

Access details: Access Details: [subscription number 907465080]

Publisher Taylor & Francis

Informa Ltd Registered in England and Wales Registered Number: 1072954 Registered office: Mortimer House, 37-41 Mortimer Street, London W1T 3JH, UK



## Philosophical Magazine

Publication details, including instructions for authors and subscription information:

<http://www.informaworld.com/smpp/title~content=t713695589>

### Scaling relationships in sharp conical indentation of shape memory alloys

Guozheng Kang<sup>a</sup>; Wenyi Yan<sup>b</sup>

<sup>a</sup> State Key Laboratory of Traction Power, Southwest Jiaotong University, Chengdu, 610031, China <sup>b</sup>

Department of Mechanical and Aerospace Engineering, Monash University, Clayton, Victoria 3800, Australia

Online publication date: 28 January 2010

**To cite this Article** Kang, Guozheng and Yan, Wenyi(2010) 'Scaling relationships in sharp conical indentation of shape memory alloys', *Philosophical Magazine*, 90: 5, 599 – 616

**To link to this Article:** DOI: 10.1080/14786430903213346

**URL:** <http://dx.doi.org/10.1080/14786430903213346>

PLEASE SCROLL DOWN FOR ARTICLE

Full terms and conditions of use: <http://www.informaworld.com/terms-and-conditions-of-access.pdf>

This article may be used for research, teaching and private study purposes. Any substantial or systematic reproduction, re-distribution, re-selling, loan or sub-licensing, systematic supply or distribution in any form to anyone is expressly forbidden.

The publisher does not give any warranty express or implied or make any representation that the contents will be complete or accurate or up to date. The accuracy of any instructions, formulae and drug doses should be independently verified with primary sources. The publisher shall not be liable for any loss, actions, claims, proceedings, demand or costs or damages whatsoever or howsoever caused arising directly or indirectly in connection with or arising out of the use of this material.

## Scaling relationships in sharp conical indentation of shape memory alloys

Guozheng Kang<sup>a</sup> and Wenyi Yan<sup>b\*</sup>

<sup>a</sup>State Key Laboratory of Traction Power, Southwest Jiaotong University, Chengdu, 610031, China; <sup>b</sup>Department of Mechanical and Aerospace Engineering, Monash University, Clayton, Victoria 3800, Australia

(Received 16 February 2009; final version received 25 July 2009)

Based on dimensional analysis and finite element calculations, several scaling relationships in the indentation of shape memory alloys with a sharp conical indenter were obtained. These scaling relationships illustrate the dependence of the indentation response on the material properties of shape memory alloys, such as phase transition and plastic deformation. It is shown that the yield stress and strain-hardening exponent of transformed martensite play important roles in the indentation response, in addition to the phase transition properties. Additionally, the general relationships between indentation hardness and phase transition stress, maximum transition strain, martensite yield stress and the strain-hardening exponent of shape memory alloys were obtained. The results show that the indentation hardness of shape memory alloys is not proportional to the phase transition stress or to the martensite yield stress, and cannot be used directly to measure the phase transition stress or the yield stress of shape memory alloys.

**Keywords:** indentation; indentation hardness; shape memory alloys; finite element modelling

### 1. Introduction

Indentation tests have been used for nearly 100 years to find the hardness of materials, and the measurement has been significantly improved in recent years due to modern indentation instruments with high precision and ease of operation. Many authors have discussed how to obtain the mechanical properties of the materials at small length scales from the load–displacement curves of micro- and nano-indentations [1,2]. For example, the hardness and Young's modulus of materials can be obtained from the peak load and the initial slope of the unloading curves [3]. More recently, indentation tests have been used to probe the mechanical properties of some advanced materials and biological materials [4–13].

---

\*Corresponding author. Email: wenyi.yan@eng.monash.edu.au

Shape memory alloys (SMAs), such as near-equiatomic NiTi alloys, have many engineering applications in micro-electro-mechanical systems, bio-medical devices and implants, seismic protection devices and aerospace structures due to their super-elasticity, shape memory effect, good biological compatibility and damping capacity [14–18]. Although the mechanical properties of bulk SMAs can be obtained from macroscopic tests, there is still a growing interest in probing their mechanical properties by micro- and nano-indentations due to its application at small scales [19–24]. However, since a phase transition from austenite to martensite and vice versa occurs in SMAs during indentation loading and unloading, the indentation of the alloys is much more complicated than that of ordinary metals without any phase transition. Some key questions need to be answered before the indentation tests are used to probe the mechanical properties of shape memory alloy. For example, are the general indentation relationships for SMAs the same as those for ordinary metals without phase transition? Can we take the indentation hardness of SMAs as a material property and deduce some mechanical properties from measuring their hardness, as in the cases of ordinary elasto-plastic and visco-elastic solids [6,25,26]? Based on dimensional analysis for the indentation hardness of ordinary metals [6,25,26], questions on spherical indentation of SMAs with a low indentation force without involving any plastic deformation of the alloys have been answered [7,8,11]. However, sharp conical indentation of SMAs has not been discussed due to the complexity caused by the plastic deformation of transformed martensite near the tip of the sharp indenter.

In this paper, we will try to answer some key questions about the indentation of SMAs with a sharp conical indenter using dimensional analysis and finite element calculations. Firstly, several scaling relationships for the indentation of SMAs with a sharp conical indenter are obtained from the dimensional analysis. Then, detailed numerical simulations are performed by the finite element method. Based on the calculated results, the effects of phase transition stress, maximum phase transition strain, martensite yield stress and the strain-hardening exponent on the maximum force and contact depth of sharp conical indentations are discussed. Finally, the quantitative relationships between the indentation hardness and phase transition and martensite plastic deformation of SMAs are illustrated in the figures obtained from our numerical simulations.

## 2. Dimensional analysis

A simple material model with strain hardening is adopted in this work for shape memory alloys. In the idealised material, the deformation of the material due to phase transition from austenite to martensite and the deformation due to the plastic yielding of the transformed martensite are described by a ‘two-step shaped’ idealised stress–strain curve under uniaxial loading, as shown in Figure 1. Following this curve from the origin, phase transition will occur when the transition stress  $\sigma_{AM}$  is reached. The maximum strain caused by complete transition is denoted by  $\varepsilon^{tr}$ . Continuous loading will result in elastic deformation of the transformed martensite until the stress reaches the yield stress of the martensite,  $\sigma_{My}$ .  $E_A$  and  $E_M$  represent the Young’s moduli of the austenite and martensite phases, respectively. Here, the

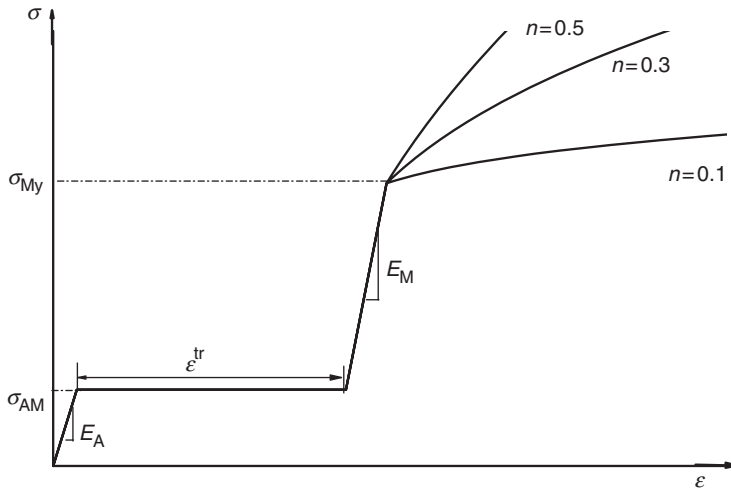


Figure 1. Idealised loading stress–strain curves of SMAs, which include martensite plastic deformation for different values of strain-hardening exponent  $n$ .

deformation due to phase transition is treated as perfect without hardening, but the plasticity of martensite is described as strain-hardening and the stress–strain curve after yielding under the uniaxial tension is described by the power law:

$$\sigma = K\varepsilon^n, \quad \text{for } \sigma \geq \sigma_{My}, \tag{1}$$

where  $K$  is the strength coefficient and  $n$  is the strain-hardening exponent. Since  $K = \sigma_{My}(E_M/\sigma_{My})^n$ , we can just use  $E_M$ ,  $\sigma_{My}$  and  $n$  to describe the stress–strain relationship of the transformed martensite.

Experimental studies have indicated that there is a certain asymmetry between tension and compression for SMAs [27]. We do not distinguish this difference in this paper for simplicity, which implies that the material under uniaxial compression is assumed to obey the idealised model as well. Considering that the material under an indenter is mainly in compression, such an assumption will not affect the results significantly. Therefore, an isotropic hardening behaviour is assumed under three-dimensional loading conditions. During the forward austenite to martensite transition process, the volume of the material reduces slightly [28,29]. This small volume change might mildly influence the mechanical behaviour of this material [30–32]. For the sake of simplicity, and considering that its value is much smaller than that of the transformation-induced shear strain, the transformation-induced volume strain is neglected in this material model. Additionally, interaction between the plastic deformation and phase transition might exist in SMAs [33,35], which is neglected in this simplified model. To include this interaction effect and the transformation-induced volume change, a much more complicated constitutive model is required. Having said that, this simplified material model can well quantify the two major deformation behaviors due to phase transition from austenite to martensite and due to plasticity of the transformed martensite, which is clearly demonstrated in published experimental papers [30,33]. Only the indentation

responses under loading, such as the maximum indentation force, ‘pile up’ or ‘sink in’ behaviours and hardness, are investigated in this paper. Therefore, there is no need to deal with the deformation behaviour under unloading, i.e. no need to consider the deformation due to reverse phase transition. Based on all these considerations and simplifications, the deformation due to phase transition during loading in the model, the ‘first step’ in Figure 1, can be treated as a special ‘plastic deformation’, which follows von Mises plasticity. It is worth mentioning that Zhang et al. [34] applied an opposite strategy to consider both phase transition and plasticity by treating plastic strain as a special ‘the strain due to phase transition’. They customised the ABAQUS build-in super-elasticity model for SMA. Similarly to our simplified model, the interaction between plastic deformation and phase transition was not considered in the Zhang et al. [34] model.

Based on the idealised material model, the dimensional analysis for the indentation response of SMAs with the plastic deformation of transformed martensite is outlined below.

For a rigid conical indenter of a given half angle  $\theta$  and a shape memory alloy idealised as shown in Figure 1, the indentation force  $F$  during loading process depends on the mechanical properties of SMAs qualified by the material parameters  $\sigma_{AM}$ ,  $\sigma_{My}$ ,  $n$ ,  $E_A$ ,  $E_M$ ,  $\nu_A$  (Poisson’s ratio of austenite),  $\nu_M$  (Poisson’s ratio of martensite) and  $\varepsilon^{tr}$ , and the geometrical parameter  $h$  (indentation depth) and  $\theta$ , as well as the coefficient of friction  $\mu$  between the indenter and the alloy, i.e.

$$F = f_L(\sigma_{AM}, \sigma_{My}, \varepsilon^{tr}, n, E_A, E_M, \nu_A, \nu_M, h, \theta, \mu). \quad (2)$$

Similarly, the contact depth  $h_c$  during the loading process can be also formulated as a function of these parameters, i.e.

$$h_c = g_L(\sigma_{AM}, \sigma_{My}, \varepsilon^{tr}, n, E_A, E_M, \nu_A, \nu_M, h, \theta, \mu). \quad (3)$$

Among these governing parameters,  $E_A$  and  $h$  have independent dimensions, and the dimensions of other parameters can be represented by the product of powers of  $E_A$  and  $h$ . Then, similar to the dimensional analysis done by Cheng and Cheng [25,26], the indentation force  $F$  and the contact depth  $h_c$  during the loading process of indentation can be written as

$$F = E_A h^2 \Pi_1 \left( \frac{\sigma_{AM}}{E_A}, \frac{\sigma_{My}}{E_A}, \varepsilon^{tr}, n, \frac{E_M}{E_A}, \nu_A, \nu_M, \theta, \mu \right) \quad (4)$$

$$h_c = h \Pi_2 \left( \frac{\sigma_{AM}}{E_A}, \frac{\sigma_{My}}{E_A}, \varepsilon^{tr}, n, \frac{E_M}{E_A}, \nu_A, \nu_M, \theta, \mu \right), \quad (5)$$

where,  $\sigma_{AM}/E_A$ ,  $\sigma_{My}/E_A$ ,  $\varepsilon^{tr}$ ,  $n$ ,  $E_M/E_A$ ,  $\nu_A$ ,  $\nu_M$ ,  $\theta$ , and  $\mu$  are dimensionless. From Equations (4) and (5), it is deduced that the dimensionless indentation force  $F/E_A h^2$  and contact depth  $h/h_c$  is independent of the indentation depth. It implies that the indentation force  $F$  is proportional to the square of the indentation depth  $h$  and the contact depth  $h_c$  is proportional to the indentation depth  $h$  in the indentation of SMAs with a sharp conical indenter. Similar conclusions have been drawn for ordinary metals [2].

For a rigid sharp conical indenter with a given half angle  $\theta$  ( $=68^\circ$ , which is used to illustrate the essential physics of conical indentation following early work [36,37]), neglecting the friction between the indenter and indented SMAs (i.e. set  $\mu=0.0$ ), the dimensionless indentation force and contact depth are the functions of parameters  $\sigma_{AM}/E_A$ ,  $\sigma_{My}/E_A$ ,  $\varepsilon^{tr}$ ,  $n$ ,  $E_M/E_A$ ,  $\nu_A$ , and  $\nu_M$ . Recent study on ordinary metals found that the friction effect can be neglected if the indenter angle is larger than  $60^\circ$  [38]. To emphasise the effects of phase transition and martensite plastic deformation on the indentation, we assume that the Young's moduli and Poisson ratios of austenite and martensite phases are, respectively, the same and  $\nu_A = \nu_M = 0.3$ . Under these conditions, the scaling relationships between the indentation force and the indentation depth and the material properties representing the phase transition and martensite plastic deformation of SMAs can be respectively simplified as

$$\frac{F}{E_A h^2} = \Pi_3 \left( \frac{\sigma_{AM}}{E_A}, \frac{\sigma_{My}}{E_A}, \varepsilon^{tr}, n \right), \quad (6)$$

$$\frac{h_c}{h} = \Pi_4 \left( \frac{\sigma_{AM}}{E_A}, \frac{\sigma_{My}}{E_A}, \varepsilon^{tr}, n \right). \quad (7)$$

When the indentation displacement reaches the maximum indentation depth, the maximum indentation force  $F_m$  and corresponding contact depth can be respectively obtained from

$$\frac{F_m}{E_A h_m^2} = \Pi_5 \left( \frac{\sigma_{AM}}{E_A}, \frac{\sigma_{My}}{E_A}, \varepsilon^{tr}, n \right) \quad (8)$$

$$\frac{h_c}{h_m} = \Pi_6 \left( \frac{\sigma_{AM}}{E_A}, \frac{\sigma_{My}}{E_A}, \varepsilon^{tr}, n \right). \quad (9)$$

### 3. Finite element simulations

Finite element simulations using ABAQUS were carried out to illustrate the scaling relationships given by Equations (8) and (9). Figure 2 shows the finite element model used in the numerical simulation, where axi-symmetrical condition was applied and  $\theta = 68^\circ$ . The size of the entire model is much larger than that of the indentation area, and the bottom of the model is constrained in both the radial and axial directions. As shown in Figure 2b, a very fine mesh with the shortest element side of  $0.1 \mu\text{m}$  is employed in the indentation area to ensure the accuracy of the numerical simulations. The number of four-noded axi-symmetrical elements used in the entire model is 2940. The yielding of transformed martensite phase obeys the von Mises yield criterion and different fixed displacement loads were applied on the rigid conical indenter. In all the calculations,  $E_A$  was taken as 50 GPa and  $\nu_A$  was 0.3.

Firstly, the linear relationships of  $F_m/E_A h_m$  versus  $h_m$  and contact depth  $h_c$  versus  $h_m$  deduced from Equations (8) and (9) are confirmed by the numerical simulations, which include the phase transition and martensite plastic deformation of SMAs.

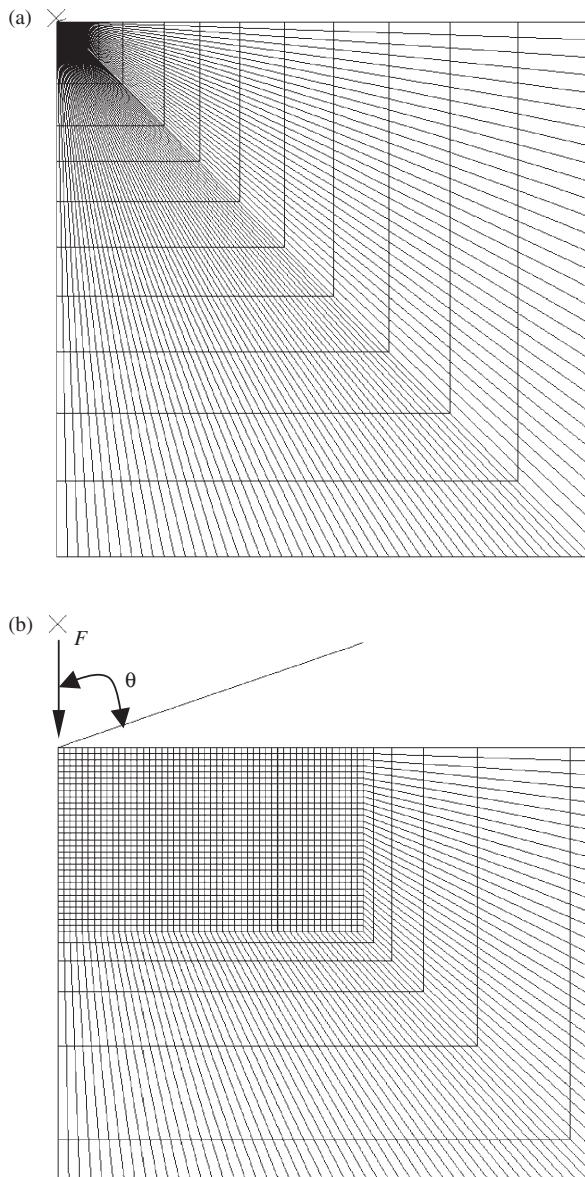


Figure 2. Finite element model for indentation simulations with a sharp conical indenter: (a) the entire model; (b) the fine mesh near the tip of the indenter.

The results are shown in Figures 3 and 4 for  $n=0.0$  and  $n \neq 0.0$ , respectively. The linear relationships hold true for all the different prescribed conditions.

Figure 5 shows the relationships of the calculated dimensionless indentation force  $F_m/E_A h_m^2$  versus the dimensionless transition stress  $\sigma_{AM}/E_A$  and the dimensionless contact depth  $h_c/h_m$  versus  $\sigma_{AM}/E_A$  for different values of the maximum transition

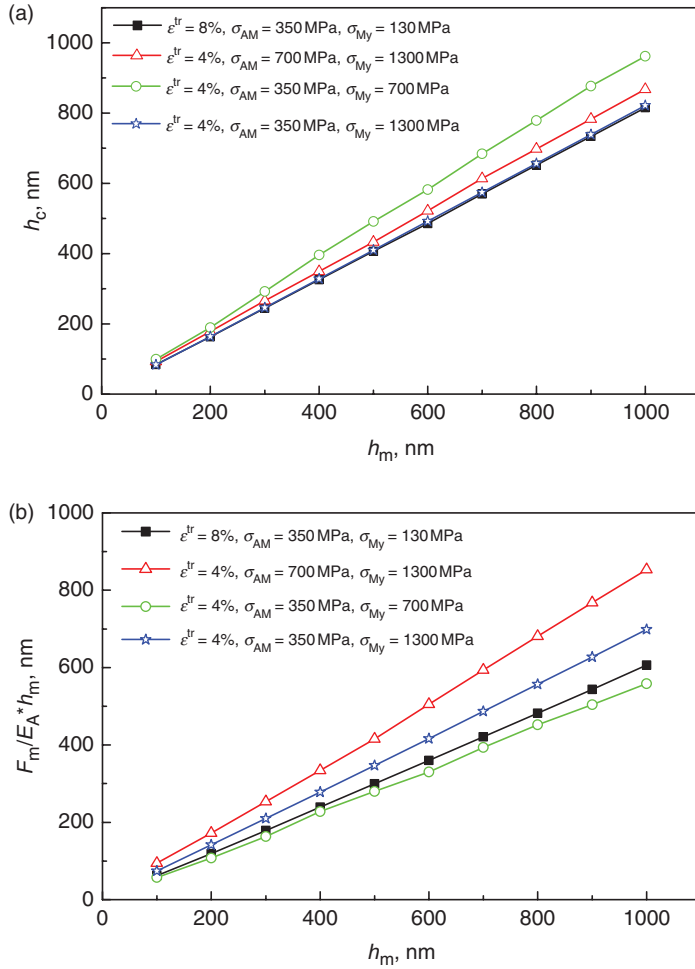


Figure 3. Simulated linear relationships between contact depth  $h_c$  and  $h_m$  (a) and between  $F_m/E_A h_m^2$  and  $h_m$  (b). ( $E_A = 50$  GPa,  $\nu_A = 0.3$ ,  $n = 0.0$ ).

strains  $\epsilon^{tr}$ , the martensite yield stresses  $\sigma_{My}$  and the strain-hardening exponents  $n$ . In the calculations, the applied maximum indentation depth  $h_m$  was set as 500 nm and the transition stress was prescribed to be less than the martensite yield stress according to the idealised stress–strain curves shown in Figure 1. It is seen that the dimensionless indentation force  $F_m/E_A h_m^2$  and the contact depth  $h_c/h_m$  increase with the increase of the transition stress  $\sigma_{AM}$ , and their values depend on the material parameters  $\epsilon^{tr}$ ,  $\sigma_{My}$  and  $n$ . However, the increasing rate of  $h_c/h_m$  becomes very small when the transition stress  $\sigma_{AM}$  closes to the martensite yield stress  $\sigma_{My}$ . Meanwhile, the effects of the maximum transition strain  $\epsilon^{tr}$  on the dimensionless indentation force  $F_m/E_A h_m^2$  and the contact depth  $h_c/h_m$  become weak as the transition stress increases. From Figure 5, it is also observed that when the martensite yield stress is low (e.g. 700 MPa), either ‘pile-up’ ( $h_c/h_m > 1$ ) or ‘sink-in’ ( $h_c/h_m < 1$ ) phenomena might

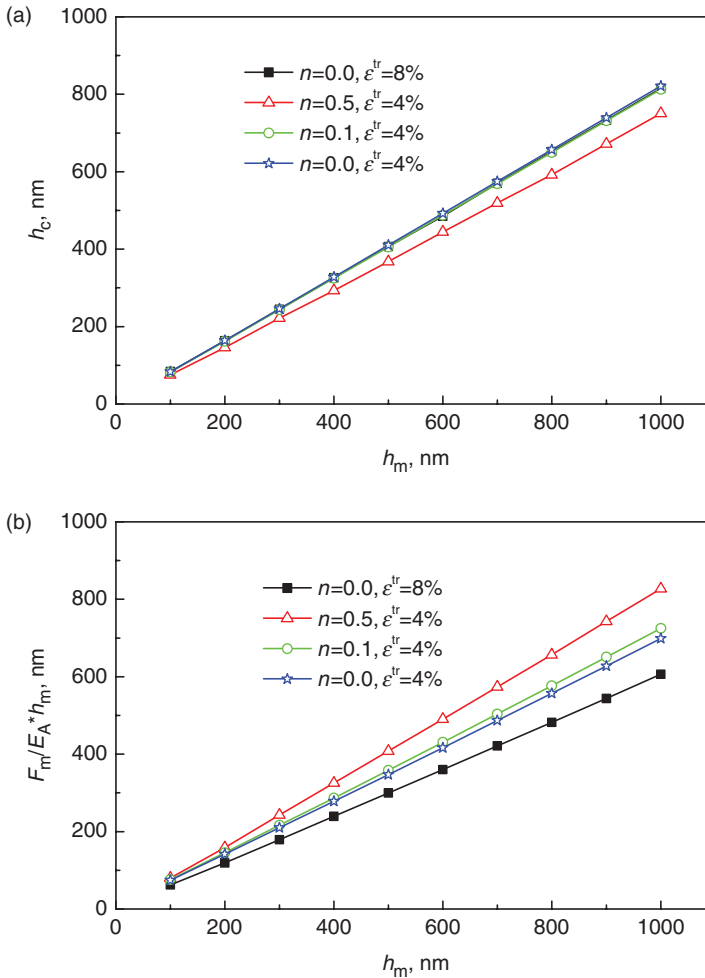


Figure 4. Simulated linear relationships between contact depth  $h_c$  and  $h_m$  (a) and between  $F_m/E_A h_m$  and  $h_m$  (b) for different values of hardening exponent  $n$  ( $E_A = 50$  GPa,  $\nu_A = 0.3$ ).

occur, which depends on the value of the transition stress. If the transition stress is low (e.g.  $\sigma_{AM}/E_A \leq 0.009$ ), ‘sink-in’ occurs; while, if the transition stress is high (e.g.  $\sigma_{AM}/E_A \geq 0.009$ ), then ‘pile-up’ takes place. This theoretical finding might be the explanation for the experimental observation that ‘pile-up’ appears at a high temperature and ‘sink-in’ appears at a low temperature in NiTi [22]. For the cases with a higher martensite yield stress (e.g.  $\sigma_{My} = 1300$  MPa), only ‘sink-in’ can be observed in the range of the prescribed transition stress.

Figure 6 displays the relationships of the calculated dimensionless indentation force  $F_m/E_A h_m^2$  versus the dimensionless yield stress  $\sigma_{My}/E_A$  and the dimensionless contact depth  $h_c/h_m$  versus  $\sigma_{My}/E_A$  for different values of strain-hardening exponent  $n$ , with a fixed maximum transition strain  $\varepsilon^{tr} (=4\%)$  and fixed transition stresses  $\sigma_{AM} (=350$  MPa). The calculated results provide a decreased relationship of the

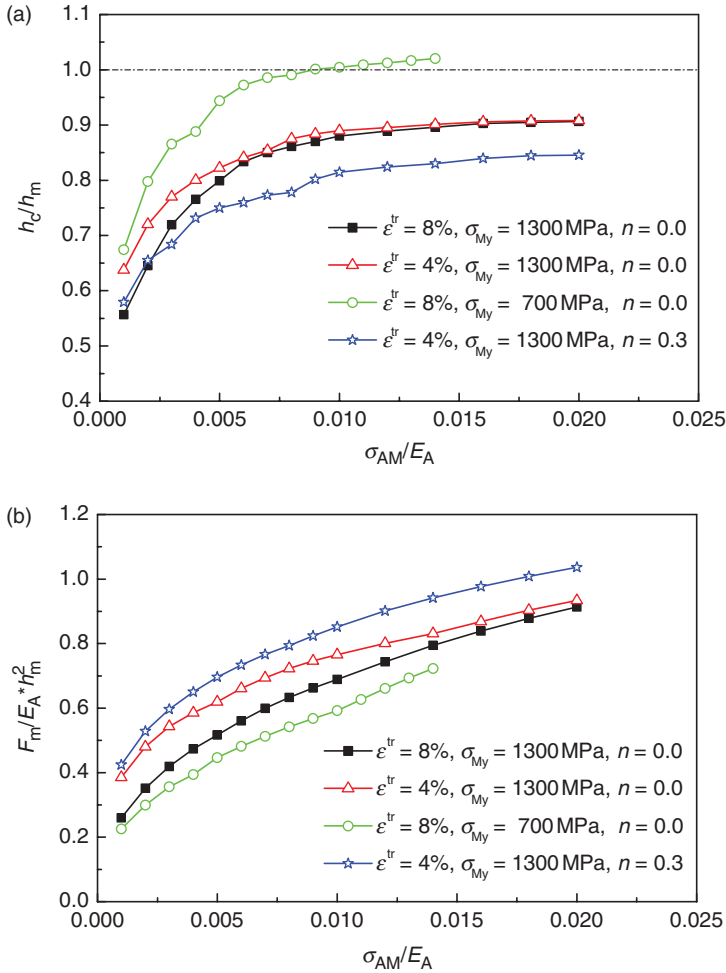


Figure 5. Simulated scaling relationships between dimensionless  $h_c/h_m$  and  $\sigma_{AM}/E_A$  (a) and between  $F_m/E_A h_m^2$  and  $\sigma_{AM}/E_A$  (b).

dimensionless contact depth  $h_c/h_m$  versus  $\sigma_{My}/E_A$  when the yield stress increases, which is different from that of the dimensionless contact depth  $h_c/h_m$  versus  $\sigma_{AM}/E_A$ . When the strain-hardening is weak (e.g.  $n = 0.0$  or  $0.1$ ), the ‘pile-up’ occurs in the range of small yield stress (e.g.  $\sigma_{My}/E_A \leq 0.013$  for  $n = 0.0$ , and  $\leq 0.0096$  for  $n = 0.1$ ), but the ‘sink-in’ takes place in the range of a high yield stress (e.g.  $\sigma_{My}/E_A > 0.015$  for  $n = 0.0$ , and  $> 0.001$  for  $n = 0.1$ ). However, for the cases of moderate and strong strain-hardening, i.e.  $n = 0.3$  and  $0.5$ , only the ‘sink-in’ appears during the indentation loading prescribed here. It is also concluded from Figure 6 that the effects of the strain-hardening exponent  $n$  on the indentation loading process decrease gradually with the increase in yield stress. These conclusions are similar to those for ordinary elasto-plastic solids with a work hardening [39].

The maximum transition strain is also a key material property of SMAs and it plays an important role in the indentation of the alloys. Its effects on the

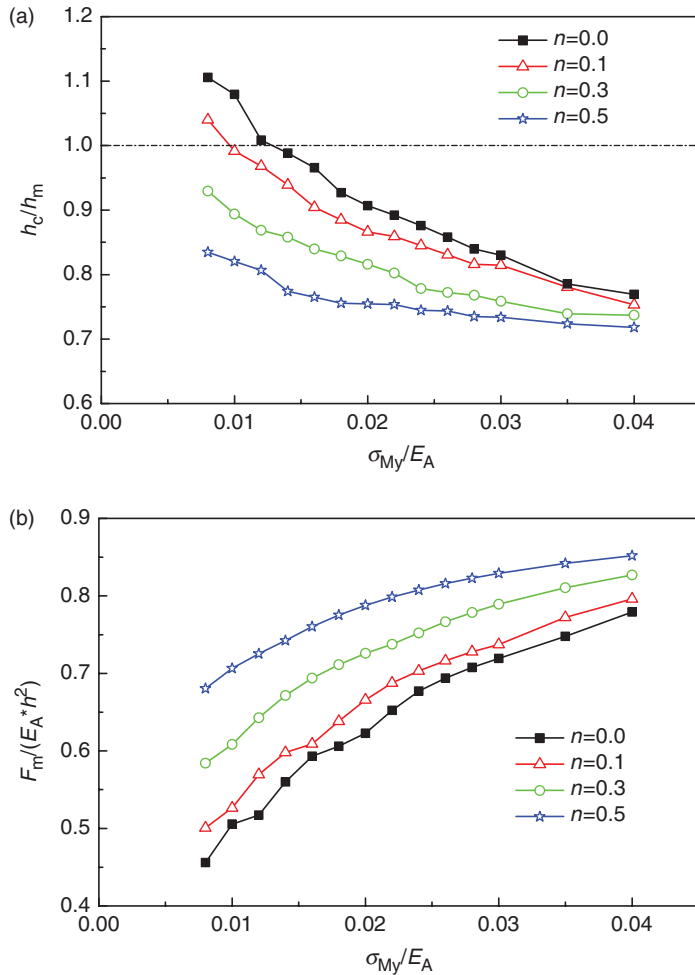


Figure 6. Simulated scaling relationships between dimensionless  $h_c/h_m$  and  $\sigma_{My}/E_A$  (a) and between  $F_m/E_A h_m^2$  and  $\sigma_{My}/E_A$  (b) for different values of strain-hardening exponent  $n$  ( $\sigma_{AM} = 350$  MPa,  $\varepsilon^{tr} = 4\%$ ).

dimensionless indentation force  $F_m/E_A h_m^2$  and the contact depth  $h_c/h_m$  have been partially displayed in Figures 3–5. Additionally, the detailed scaling relationships of the calculated dimensionless indentation force  $F_m/E_A h_m^2$  versus the maximum transition strain  $\varepsilon^{tr}$  and the dimensionless contact depth  $h_c/h_m$  versus  $\varepsilon^{tr}$  for different values of yield stress  $\sigma_{My}$  and hardening exponent  $n$ , with a fixed transition stresses  $\sigma_{AM}$  ( $=350$  MPa) are shown in Figure 7. The simulated results indicate that the variation of the maximum transition strain hardly affects the dimensionless contact depth  $h_c/h_m$  (Figure 7a), but the increase of the maximum transition strain results in a clear decrease of dimensionless indentation force  $F_m/E_A h_m^2$ , especially for the case with a high yield stress and a moderate or strong hardening (Figure 7b).

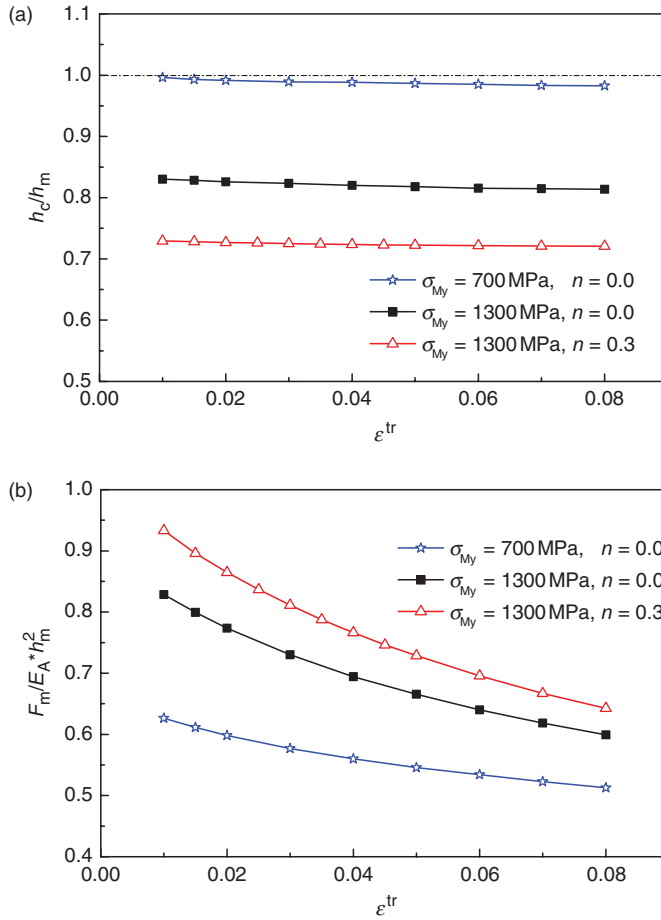


Figure 7. Simulated scaling relationships between the dimensionless  $h_c/h_m$  and  $\epsilon^{tr}$  (a) and between  $F_m/E_A h_m^2$  and  $\epsilon^{tr}$  (b) for different values of yield stress  $\sigma_{My}$  and hardening exponent  $n$  ( $\sigma_{AM} = 350 \text{ MPa}$ ).

#### 4. Indentation hardness of shape memory alloys

As Cheng and Cheng [25] defined the indentation hardness of ordinary elasto-plastic solids, the hardness of SMAs with a sharp conical indenter can be evaluated as

$$H = \frac{F_m}{A_m} = \frac{F_m}{\pi h_c^2|_{h=h_m} \tan^2 \theta}, \quad (10)$$

where  $A_m$  is the projected contact area when the indentation force reaches its maximum  $F_m$ . Using the scaling relationships of the indentation force and the contact depth Equations (8) and (9) and considering  $\theta$  is a constant, we can deduce the scaling relationship of the indentation hardness  $H/E_A$  as

$$\frac{H}{E_A} = \frac{F_m}{E_A A_m} = \Pi_7 \left( \frac{\sigma_{AM}}{E_A}, \frac{\sigma_{My}}{E_A}, \epsilon^{tr}, n \right). \quad (11)$$

It implies that the indentation hardness of SMAs with a given conical indenter depends on the transition stress  $\sigma_{AM}$ , the maximum transition strain  $\varepsilon^{tr}$ , the martensite yield stress  $\sigma_{My}$  and the strain-hardening exponent  $n$ , if the friction is neglected and the other material parameters are set as constant.

To compare the results of SMAs with those of ordinary metals, the following two scaling relationships are also derived:

$$\frac{H}{\sigma_{AM}} = \frac{E_A}{\sigma_{AM}} \Pi_7 \left( \frac{\sigma_{AM}}{E_A}, \frac{\sigma_{My}}{E_A}, \varepsilon^{tr}, n \right) \quad (12)$$

$$\frac{H}{\sigma_{My}} = \frac{E_A}{\sigma_{My}} \Pi_7 \left( \frac{\sigma_{AM}}{E_A}, \frac{\sigma_{My}}{E_A}, \varepsilon^{tr}, n \right). \quad (13)$$

Based on the numerical results from the finite element calculations, the quantitative relationships between the hardness and the phase transition stress  $\sigma_{AM}$ , the maximum transition strain  $\varepsilon^{tr}$ , the martensite yield stress  $\sigma_{My}$  and the hardening exponent  $n$  are presented below.

Figure 8 shows the relationships between the calculated dimensionless indentation hardness  $H/E_A$  and the dimensionless transition stress  $\sigma_{AM}/E_A$  for different values of martensite yield stress  $\sigma_{My}$  and hardening exponent  $n$ . It is seen that when the transition stress  $\sigma_{AM}$  is very small (e.g.  $\sigma_{AM}/E_A < 0.005$  for the cases with martensite yield stress  $\sigma_{My} = 1300$  MPa), the indentation hardness slightly decreases with the increase in  $\sigma_{AM}$ . After that, the hardness increases monotonically with  $\sigma_{AM}$ . The  $\sigma_{AM}/E_A$  value of the turning point varies from 0.008 to 0.003 depending on the prescribed value of martensite yield stress  $\sigma_{My}$  (for NiTi shape memory alloys, its reasonable value ranges from 500 to 1800 MPa depending on the thermal treatment of the alloys). Experimental study [10] found an anomalous increased

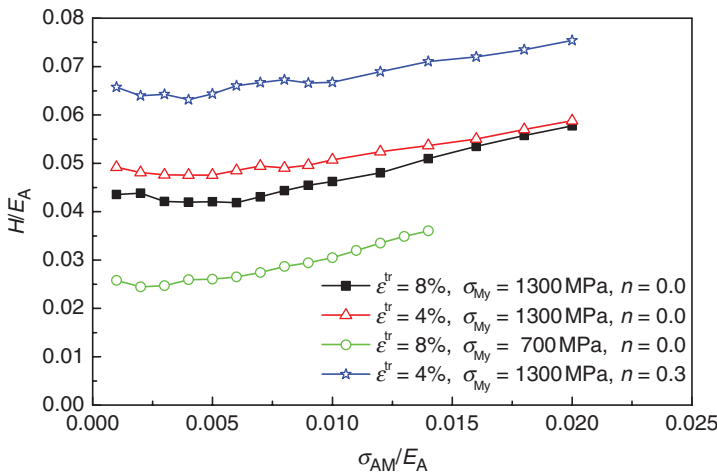


Figure 8. Relationships between dimensionless hardness  $H/E_A$  and dimensionless phase transition stress  $\sigma_{AM}/E_A$  for different values of yield stress  $\sigma_{My}$ , hardening exponent  $n$  and maximum transition strain  $\varepsilon^{tr}$ .

hardness of super-elastic NiTi shape memory alloy when the ambient temperature changes from 22 to 120°C, which corresponds to the increase in the phase transition stress from near 400 to 1000 MPa, while the martensite yield stress is almost unchanged (about 1600 MPa) within this range of temperature. The influence of the phase transition stress on the hardness shown in Figure 8 (in the range of  $\sigma_{AM}/E_A > 0.005$ ) qualitatively explains this experimental finding.

The maximum transition strain  $\varepsilon^{tr}$  indicates the degree of phase transition in shape memory alloys. However, its effect on the indentation hardness of NiTi SMAs was not investigated in [10], while their experimental data showed a decreased maximum transition strain at elevated temperatures. Using the finite element method, the relationships between the hardness and maximum transition strain are obtained for different values of martensite yield stress  $\sigma_{My}$  and hardening exponent  $n$ , with a fixed transition stress  $\sigma_{AM} = 350$  MPa. The calculated results in Figure 9 show that, if the transition stress and martensite yield stress are constant, a decreased maximum transition strain results in increased indentation hardness, especially for the cases with higher values of martensite yield stress and hardening exponent. It implies that the effect of maximum transition strain on hardness is more obvious in cases with a high yield stress and a strong strain hardening. Figure 8 also illustrates that the effect of maximum transition strain on indentation hardness of shape memory alloy depends on the value of the transition stress. When the transition stress is relatively higher and closer to the martensite yield stress, the variation in maximum transition strain hardly influences the hardness value. Therefore, it is concluded that the anomalous increased hardness of super-elastic NiTi alloy observed in the experimental study [10] is caused by both increased transition stress and decreased maximum transition strain as the ambient temperature is elevated, and the transition stress becomes a dominated factor as the transition stress is close to the martensite yield stress.

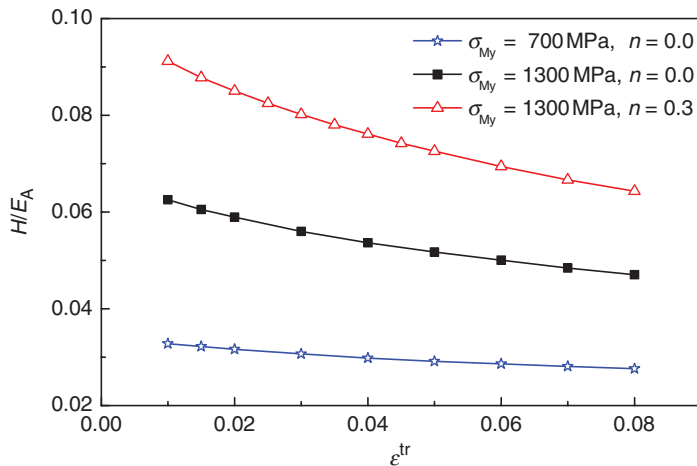


Figure 9. Relationships between dimensionless hardness  $H/E_A$  and maximum phase transition strain  $\varepsilon^{tr}$  for different values of yield stress  $\sigma_{My}$  and hardening exponent  $n$  ( $\sigma_{AM} = 350$  MPa).

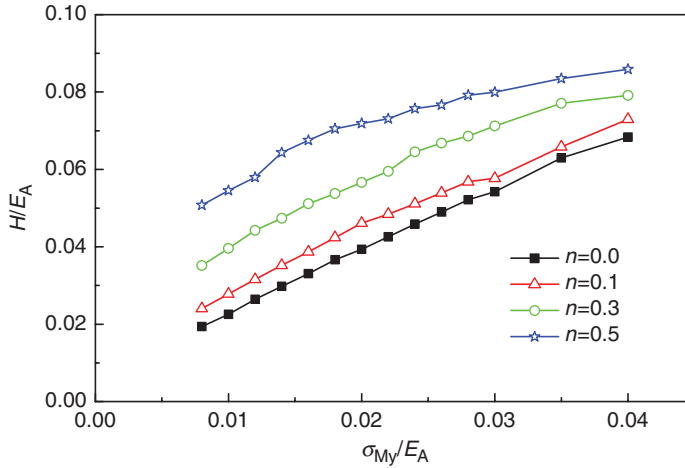


Figure 10. Relationships of dimensionless hardness  $H/E_A$  versus dimensionless martensite yield stress  $\sigma_{My}/E_A$  with several hardening exponents  $n$  ( $\sigma_{AM} = 350$  MPa,  $\varepsilon^{tr} = 4\%$ ).

In addition to the phase transition, the plastic deformation of the transformed martensite phase also affects the indentation hardness of SMAs with a sharp conical indenter, as outlined in Figures 8 and 9. Here, more detailed relationships between the dimensionless hardness and martensite yield stress are provided in Figure 10 for several values of the hardening exponent ranging from weak to strong strain hardening. We can observe from Figure 10 that hardness increases with the increase in yield stress and hardening exponent, and the effect of the hardening exponent on hardness decreases with the increase in yield stress. The calculation with a very high yield stress (e.g.  $\sigma_{My}/E_A > 0.08$ ) shows that the variation in hardening exponent hardly affects the value of the hardness, and the yield stress becomes the only dominated factor; however, such a high value of yield stress is not practical for SMAs. In the reasonable range of yield stress, the strain hardening plays an important role in determining the hardness of SMAs. These conclusions are similar to those for ordinary metals [2,39].

For ordinary perfectly elasto-plastic solids, Cheng and Cheng [25] demonstrated that the ratio of hardness  $H$  to Young's modulus  $E$  almost remains constant between 2.5 and 2.6 when the normalised yield stress  $\sigma_y/E$  changes in the reasonable range of  $0 < \sigma_y/E < 0.01$  ( $E = 100\text{--}200$  GPa). However, our previous work [40] concerning a perfect plastic deformation of martensite phase showed that the ratio of the indentation hardness to the martensite yield stress does not remain unchanged even in the range of  $0 \leq \sigma_{My}/E_A \leq 0.01$ , and it decreases continuously with the increase in normalised yield stress  $\sigma_{My}/E_A$  of SMAs. What will the results be for the cases with strain hardening?

Figures 11 and 12 give the calculated relationships between the normalised hardness  $H/\sigma_{AM}$  and the normalized transition stress  $\sigma_{AM}/E_A$ , between the normalised hardness  $H/\sigma_{My}$  and the yield stress  $\sigma_{My}/E_A$ , respectively, for different values of hardening exponent  $n$  ranging from weak to strong strain hardening. It is shown that the indentation hardness of SMAs is not proportional to the

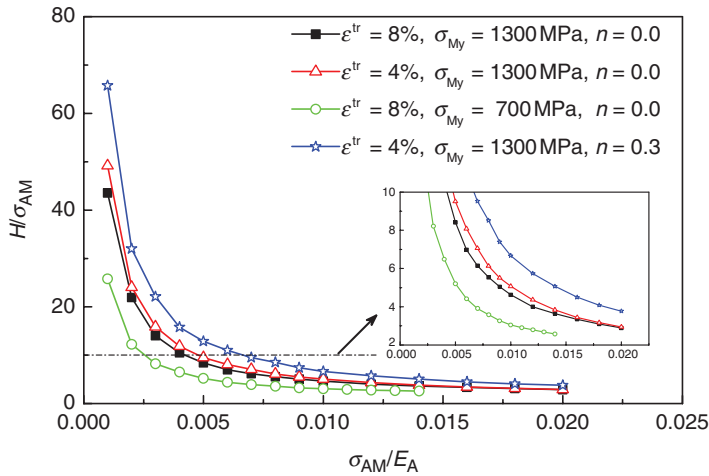


Figure 11. Relationships between dimensionless hardness  $H/\sigma_{AM}$  and dimensionless phase transition stress  $\sigma_{AM}/E_A$ .

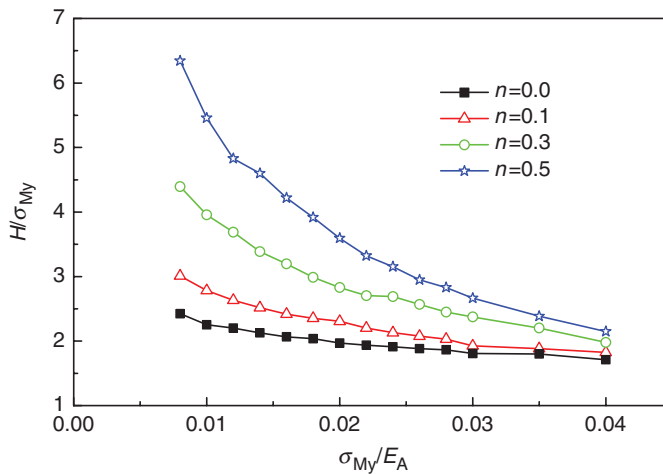


Figure 12. Relationships between dimensionless hardness  $H/\sigma_{My}$  and dimensionless martensite yield stress  $\sigma_{My}/E_A$  for different values of hardening exponent  $n$ .

transition stress or to the martensite yield stress. The ratios of indentation hardness to transition stress and to yield stress decrease continuously with the increase in transition stress and with the increase in yield stress, respectively, even if the transition stress is close to the prescribed martensite yield stress and the yield stress is small. In the range of small yield stress and small transition stress, the normalised hardness ( $H/\sigma_{AM}$  or  $H/\sigma_{My}$ ) of the alloys with a strong strain hardening is many times that of the alloys without strain hardening, and the hardening exponent  $n$  plays an important role in determining the normalised hardness of the alloys; however, the effect of strain hardening on the normalised hardness of the alloys

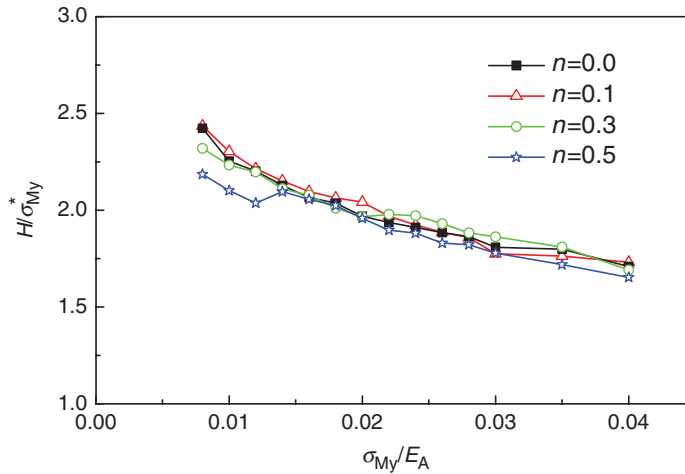


Figure 13. Relationships between dimensionless hardness  $H/\sigma_{My}^*$  and dimensionless martensite yield stress  $\sigma_{My}^*/E_A$ .  $\sigma_{My}^*$  is the yield stress at the representative strain of 0.1.

becomes much weaker when the yield stress and the transition stress are higher. We can conclude that the hardness of SMAs is not proportional to the martensite yield stress or to the transition stress, even within the range of small yield stress values. The hardness cannot be simply used as a measure of the phase transition stress or plastic yield stress, which is in contrast to ordinary metals.

For ordinary elasto-plastic materials, the hardening exponent will also affect the ratio of hardness to initial yield strength for a small ratio of initial yield strength to the Young's modulus [2]. However, if one chooses the strength at a representative strain, Cheng and Cheng [2] found that the influence of the hardening exponent on the ratio of hardness to yield stress at the representative strain can be neglected. Following this idea, we re-plotted Figure 12 by normalising the hardness value by the yield stress at a representative strain of 0.1, which is a total strain including elastic strain, phase transition strain and plastic strain. The new curves are shown in Figure 13. Now the four curves merge into one curve, which indicates that the influence of the hardening exponent on the new normalised hardness can be neglected. This conclusion is consistent with ordinary metals.

## 5. Conclusions

From scaling analysis and finite element calculations, several dimensionless relationships were obtained for SMAs with solid phase transition. The relationships display the dependence of the indentation force  $F$ , the contact depth  $h_c$  and the indentation hardness  $H$  in a sharp conical indentation upon the material properties of SMAs. This represents the phase transition and the plastic deformation of the transformed martensite phase, i.e. the transition stress  $\sigma_{AM}$ , the maximum transition strain  $\epsilon^{tr}$ , the martensite yield stress  $\sigma_{My}$  and the strain hardening exponent  $n$ . The results show that, even for SMAs, including the plastic deformation of

transformed martensite, the linear relationships of  $F_m/E_A h_m$  versus  $h_m$  and  $h_c$  versus  $h_m$  hold true, and the indentation hardness of SMAs is independent of indentation depth. Surely, the values of the dimensionless indentation force  $F_m/E_A h_m^2$ , the contact depth  $h_c/h_m$  and the indentation hardness  $H/E_A$  change with the values of the transition stress  $\sigma_{AM}$ , the maximum transition strain  $\epsilon^{tr}$ , the martensite yield stress  $\sigma_{My}$  and the strain hardening exponent  $n$ . A higher transition stress or a higher martensite yield stress or a lower maximum transition strain would lead to a higher indentation hardness, which is in agreement with the experimental measurement [10] and a previous study on spherical indentation hardness [11]. A higher strain hardening would also result in a higher indentation hardness. The results further indicate that the ratio of hardness to the phase transition stress or to the plastic yield stress is not a constant; it decreases continuously with an increase in the corresponding stress value. The hardness cannot be simply used as a measure of phase transition stress or plastic yield stress of transformed martensite phase, which is in contrast to ordinary metals.

### Acknowledgements

The authors are grateful to the two reviewers for their constructive comments for improving the article. This study is supported by the Program for New Century Excellent Talents at University (NCET 05-0796) of China. GK acknowledges his visiting academic residency at Monash University on the invitation by WY.

### References

- [1] D. Tabor, *Phil. Mag.* A 74 (1996) p.1207.
- [2] Y.T. Cheng and C.M. Cheng, *Mater. Sci. Eng. R* 44 (2004) p.91.
- [3] W.C. Oliver and G.M. Pharr, *J. Mater. Res.* 7 (1992) p.1564.
- [4] K. Tunvisut, E.P. Busso, N.P. O'Dowd and H.P. Brantner, *Phil. Mag.* A 82 (2002) p.2013.
- [5] Z.H. Xu and J. Agren, *Phil. Mag.* 84 (2004) p.2367.
- [6] Y.T. Cheng and C.M. Cheng, *Mater. Sci. Eng. A* 409 (2005) p.93.
- [7] W. Yan, Q. Sun, X.-Q. Feng and L. Qian, *Appl. Phys. Lett.* 88 (2006) p.241912.
- [8] W. Yan, Q. Sun and H.-Y. Liu, *Mater. Sci. Eng. A* 425 (2006) p.278.
- [9] D.M. Ebenstein and L.A. Pruitt, *Nanotoday* 1 (2006) p.26.
- [10] L. Qian, Q. Sun and X.D. Xiao, *Wear* 260 (2006) p.509.
- [11] W. Yan, Q. Sun, X.-Q. Feng and L. Qian, *Int. J. Solid. Struct.* 44 (2007) p.1.
- [12] S. Guicciardi and G. Pezzotti, *J. Ceram. Soc. Jpn.* 115 (2007) p.186.
- [13] X.-Q. Feng, L. Qian, W. Yan and Q. Sun, *Appl. Phys. Lett.* 92 (2008) p.121909.
- [14] T.W. Duering, K.N. Melton, D. Stoekel and C.M. Wayman, *Engineering Aspects of Shape Memory Alloys*, Butterworth-Heinemann, London, 1990.
- [15] K. Otsuka and C.M. Wayman, *Shape Memory Materials*, Cambridge University Press, Cambridge, 1998.
- [16] K. Otsuka and X. Ren, *Intermetallics* 7 (1999) p.511.
- [17] M. Dolce and D. Cardone, *Int. J. Mech. Sci.* 43 (2001) p.2631.
- [18] Y. Fu, H. Du, W. Huang, S. Zhang and M. Hu, *Sens. Actuat. A* 112 (2004) p.395.
- [19] R. Liu and D.Y. Li, *Mater. Sci. Tech. Lond.* 16 (2000) p.328.
- [20] F.T. Cheng, P. Shi and H.C. Man, *Scripta Mater.* 45 (2001) p.1083.

- [21] K. Gall, K. Juntunen, H.J. Maier, H. Sehitoglu and Y.I. Chumlyakov, *Acta Mater.* 49 (2001) p.3205.
- [22] W.M. Huang, J.F. Su, M.H. Hong and B. Yang, *Scripta Mater.* 53 (2005) p.1055.
- [23] L.M. Qian, X.D. Xiao, Q. Sun and T.X. Yu, *Appl. Phys. Lett.* 84 (2004) p.1076.
- [24] W. Ni, Y.T. Cheng and D.S. Grummon, *Appl. Phys. Lett.* 82 (2003) p.2811.
- [25] Y.T. Cheng and C.M. Cheng, *Int. J. Solid. Struct.* 36 (1999) p.1231.
- [26] Y.T. Cheng and C.M. Cheng, *Surf. Coat. Tech.* 133–134 (2000) p.417.
- [27] C.P. Frick, A.M. Ortega, J. Tyber, K. Gall and A.J. Maier, *Metall. Mater. Trans. A* 35 (2004) p.2013.
- [28] D.-N. Fang, W. Lu, W. Yan, T. Inoue and K.-C. Hwang, *Acta Mater.* 47 (1998) p.269.
- [29] R.L. Holtz, K. Sadananda and M.A. Imam, *Int. J. Fatigue* 21 (1999) p.s137.
- [30] A.L. McKelvey and R.O. Ritchie, *Metall. Mater. Trans. A* 32 (2001) p.731.
- [31] W. Yan, C.H. Wang, X.P. Zhang and Y.-W. Mai, *Smart Mater. Struct.* 11 (2002) p.947.
- [32] W. Yan, Q. Sun and H.-Y. Liu, *Int. J. Mod. Phys. B* 22 (2008) p.5957.
- [33] A.L. McKelvey and R.O. Ritchie, *J. Biomed. Mater. Res.* 47 (1999) p.301.
- [34] Y. Zhang, Y.-T. Cheng and D.S. Grummon, *J. Appl. Phys.* 101 (2007) p.053507.
- [35] W. Yan, C.H. Wang, X.P. Zhang and Y.-W. Mai, *Mater. Sci. Eng. A* 354 (2005) p.146.
- [36] A.K. Bhattacharya and W.D. Nix, *Int. J. Solid. Struct.* 24 (1998) p.881.
- [37] Y.T. Cheng, Z.Y. Li and C.M. Cheng, *Phil. Mag. A* 82 (2002) p.1821.
- [38] J.L. Bucaille, S. Stauss, E. Felder and J. Michler, *Acta Mater.* 51 (2003) p.1663.
- [39] Y.T. Cheng and C.M. Cheng, *Appl. Phys. Lett.* 73 (1998) p.614.
- [40] G.Z. Kang and W. Yan, *Appl. Phys. Lett.* 94 (2009) p.261906.